

Key parameter estimation for radar rotating object imaging with multi-aspect observations

YE ChunMao, XU Jia*, PENG YingNing & WANG XiuTan

Department of Electronic Engineering, Tsinghua University, Beijing 100084, China

Received October 9, 2008; accepted January 18, 2010

Abstract Rotating object model is commonly used for imaging analysis in high resolution radars such as the inverse synthetic aperture radar (ISAR). For a rotating object, it is known that multi-aspect observations can improve cross-range resolution with the known imaging geometry. For the non-cooperative rotating object with unknown imaging geometry, this paper proposes an integrated scheme to estimate the key parameters, e.g., the rotating velocity and the aspect angle difference between every two observations. Furthermore, convolution back-projection (CBP) method is applied to provide fused imaging result with improved resolution. Also, the accuracy of the ultimate parameter estimation is analyzed, which is strongly related with several important factors like position extraction error of scattering centers and so on. Finally, the results of numerical experiments are provided to demonstrate the effectiveness of the proposed method.

Keywords rotating objects, multi-aspect observations, fused imaging, aspect angle difference

Citation Ye C M, Xu J, Peng Y N, et al. Key parameter estimation for radar rotating object imaging with multi-aspect observations. *Sci China Inf Sci*, 2010, 53: 1641–1652, doi: 10.1007/s11432-010-4028-3

1 Introduction

After effective translational motion compensation, a target or a scene with limited size is commonly viewed as a rotating object by some high resolution radars such as the inverse synthetic aperture radar (ISAR) [1]. Usually, ISAR obtains high resolution of a target along the radar line of sight (RLOS) direction by processing wideband echoes and further obtains high resolution perpendicular to RLOS, i.e., in the cross-range direction, by coherently accumulating a number of echoes from different observation aspects. Thus, a 2D imaging result is obtained that may help the awareness of the target [1–3]. According to the ISAR imaging theory, the resolution along RLOS can be improved by signals with larger bandwidth, and the cross-range resolution can be improved by wider aspect observations. It is known that high resolution imaging results of multi-aspect can improve the performance of target identification [4]. Also, observations from multi-aspect can be used to form 2D images with better resolution [5] or to perform 3D reconstruction of a target [6–8], and enable more reliable target identification [6]. Thus, how to exploit multi-aspect observations becomes an important problem for new radar systems such as the multi-channel, multi-static and netted radar imaging systems.

Usually, wide aspect observation of a rotating object can be obtained with two methods. The first method is to perform long time observation with a monostatic ISAR [6], and the second method is

*Corresponding author (email: xujia@mail.tsinghua.edu.cn)

to obtain multi-aspect observation in a short time with multiple radar receivers deployed at different locations. However, the feasibility of the first method is usually weak for a non-cooperative moving target. At the cost of increase in hardwares, multiple receivers can be deployed at different locations to perform multi-aspect observations for a target in a limited observation interval. There are plenty of ways to deploy multiple receivers for different applications. For example, Martorella et al. [9–11] proposed a configuration with two radar transceivers to simultaneously obtain the monostatic and bistatic observation of a target. The fused imaging with data collected by multiple receivers is much more complicated than the monostatic ISAR imaging. Firstly, the unknown motion of the target bothers the multi-aspect imaging process just as in the monostatic ISAR imaging process. Secondly, the imaging geometry is unknown for multi-aspect observations. In other words, the data collection surfaces may not be planar, and their relations are unknown. Besides, different fusion schemes are required for different imaging occasions. As is known, one fused imaging scheme can provide ISAR images with higher resolution when the data collection surfaces are coplanar, and another fused imaging scheme can provide 3D reconstruction of a target when the data collection surfaces are not coplanar. At present, the research on rotating object imaging with multi-aspect observations is at the beginning stage. Li et al. [5] proposed a fused imaging scheme for ISAR targets with data collected from different aspects with known imaging geometry. Researchers have discussed 3D reconstruction of an ISAR target by different means, such as exploiting 2D ISAR image sequences, and establishing new ISAR configurations with multiple receivers or interferometric processing.

For rotating object imaging with multiple coplanar observations, an integrated scheme is proposed in this paper to estimate the rotational motion of a target as well as the aspect angle difference (AAD) between every two observations, so as to provide fused imaging results with higher resolution. This paper takes the configuration of two ISAR systems as an example to demonstrate the effectiveness of the proposed method. With this proposed method, range Doppler (RD) images of a target are formed at first with data collected from different aspect angles. Then, prominent scattering centers are extracted from different RD images to estimate the required imaging geometry information for the successive fused imaging process. Notably, this proposed method is also suitable for multi-aspect coplanar observations.

2 Imaging geometry of two-aspect observations

In this paper, the well-known rotating object model is adopted, which has two radars for transmitting orthogonal waveform, and deployed at (R_{AO}, β_A) and (R_{BO}, β_B) (see Figure 1(a)). Further, suppose that these two radars transmitting signals with the same bandwidth and carrier frequency, and the target rotating with a constant velocity of ω_o . Under far-field conditions, the distance from a prominent scatter center $P(r_o, \theta_o)$ on this target to radar A varies with the pulse time t_m as

$$R_A = \sqrt{R_{AO}^2 + r_o^2 - 2R_{AO}r_o \cos(\theta_o + \theta_A(t_m))} \approx R_{AO} - r_o \cos(\theta_o + \theta_A(t_m)), \quad (1)$$

where $\theta_A(t_m) = \omega_o t_m - \beta_A$ is the pulse time varied aspect angle of radar A.

As we known, the RD imaging of a rotating object actually measures the time delay and Doppler of a scattering center. Thus, a scattering center is mapped on the RD plane

$$X_A(t_m) = -f_s \frac{2R_A}{c} \approx X_{AO} + \frac{r_o}{\eta_r} \cos(\theta_o + \theta_A(t_m)), \quad (2)$$

$$Y_A(t_m) = \frac{M}{f_r} \frac{2}{\lambda} \frac{dR_A}{dt_m} \approx \frac{r_o \sin(\theta_o + \theta_A(t_m))}{\eta_a}, \quad (3)$$

where f_s is the sampling frequency, c is the velocity of light, f_r is the pulse repetition frequency, λ is the wavelength, M is the number of accumulated pulses, $X_{AO} = -R_{AO}/\eta_r$ is a constant term, $\eta_r = c/(2f_s)$ and $\eta_a = \lambda f_r/(2M\omega_o)$ are the range and cross-range scaling factors, respectively.

The RD mapping in eqs. (2) and (3) is further rewritten in the matrix form as

$$\begin{bmatrix} X_A(t_m) \\ Y_A(t_m) \end{bmatrix} = \begin{bmatrix} X_{AO} \\ 0 \end{bmatrix} + \mathbf{SR}_A(t_m) \begin{bmatrix} x_o \\ y_o \end{bmatrix}, \quad (4)$$

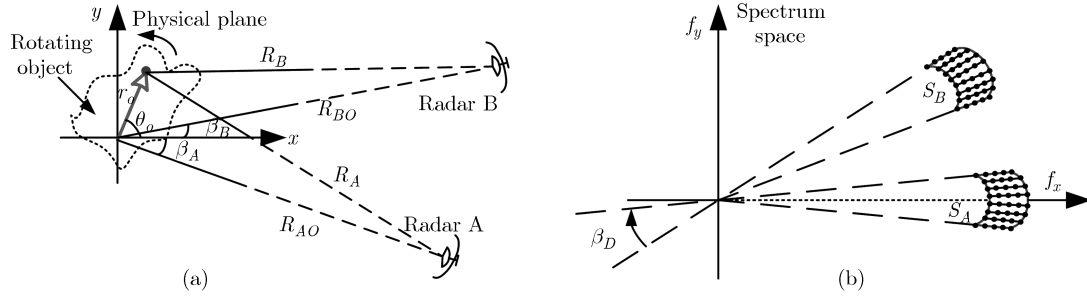


Figure 1 Imaging configuration. (a) Imaging geometry; (b) data supporting area.

where S is the scaling matrix and R_A is the pulse time varied aspect matrix of radar A,

$$S = \begin{bmatrix} 1/\eta_r & \\ & 1/\eta_a \end{bmatrix}, \quad R_A(t_m) = \begin{bmatrix} \cos \theta_A(t_m) & -\sin \theta_A(t_m) \\ \sin \theta_A(t_m) & \cos \theta_A(t_m) \end{bmatrix}. \quad (5)$$

Also, this scattering center is mapped on the RD image form by radar B at

$$\begin{bmatrix} X_B(t_m) \\ Y_B(t_m) \end{bmatrix} = \begin{bmatrix} X_{BO} \\ 0 \end{bmatrix} + SR_B(t_m) \begin{bmatrix} x_o \\ y_o \end{bmatrix}, \quad (6)$$

where $\theta_B(t_m) = \omega_o t_m - \beta_B$ is the pulse time varied aspect angle for radar B, and $X_{BO} = -R_{BO}/\eta_r$ is a constant term, and R_B is the corresponding aspect matrix.

$$R_B(t_m) = \begin{bmatrix} \cos \theta_B(t_m) & -\sin \theta_B(t_m) \\ \sin \theta_B(t_m) & \cos \theta_B(t_m) \end{bmatrix}. \quad (7)$$

3 Fused imaging principle

From the imaging geometry in Figure 1(a) and after omitting the amplitude terms, the phase history of received echoes by radar A is expressed as

$$\begin{aligned} G_A(f, t_m) &= \int_{-\infty}^{\infty} \int_{-\infty}^{\infty} \rho(x, y) \exp\{j2\pi K Q_A(t_m)\} dx dy \\ &= \int_{-\infty}^{\infty} \int_{-\infty}^{\infty} \rho(x, y) \exp[j2\pi(x f_x + y f_y)] dx dy, \end{aligned} \quad (8)$$

where $Q_A(t_m) = r \cos(\theta + \theta_A(t_m))$ is the projection of the scattering center's position vector on the RLOS of radar A, $K = 2f/c$ is the wavenumber, $f = f_b + f_c$, f_b is the baseband frequency, f_c is the carrier frequency, $x = r \cos(\theta - \beta_A)$ and $y = r \sin(\theta - \beta_A)$ defines the physical plane of radar A, $\rho(x, y)$ is the 2D scattering function of the target, $f_x = K \cos(\omega_o t_m)$ and $f_y = -K \sin(\omega_o t_m)$ defines the spectrum space.

Let $\beta_D = \beta_A - \beta_B$ denote the AAD between the RLOS of radar A and radar B, and u and v define the physical plane of radar B. Then the physical planes of radar A and radar B can be related by

$$\begin{bmatrix} u \\ v \end{bmatrix} = \begin{bmatrix} \cos \beta_D & -\sin \beta_D \\ \sin \beta_D & \cos \beta_D \end{bmatrix} \begin{bmatrix} x \\ y \end{bmatrix}. \quad (9)$$

By eq. (9), the target has different poses on the RD image planes of radar A and radar B, and the pose difference is determined by the AAD of two radar's RLOS.

In real applications, the bandwidth of radar systems and the observed aspect angles are both limited. Thus, the supporting area of the received data by two ISAR systems is also limited as shown in Figure

1(b). To produce a fused image with higher resolution, the received data of two ISAR systems should be coherently accumulated [5],

$$g(x, y) = \int \int G_A(f, t_m) \exp[-j2\pi(xf_x + yf_y)] dS_A + T_f \left\{ \int \int G_B(f, t_m) \exp[-j2\pi(uf_x + vf_y)] dS_B \right\}, \quad (10)$$

where S_A and S_B denote the supporting area of received data by radar A and radar B, respectively, $T_f(\cdot)$ denotes the transformation from (u, v) to (x, y) . Notably, the above integration process can be accomplished through the convolution back-projection (CBP) [12].

According to the above analysis, the information of the equivalent rotational motion of the target and the AAD between each data collection plane should be provided first to produce a fused image with multi-aspect observations.

4 Target's rotation and AAD estimation

To provide the required information for fused imaging, this section proposes an integrated scheme to estimate the equivalent rotating velocity, rotating center of the target, and the AAD between every two data collection planes by extracting prominent scattering centers on the RD images of each aspect. Then, with the CBP algorithm, a fused imaging result is obtained.

Suppose that the sub-pixel level positions of three scattering centers (x_i, y_i) , (x_k, y_k) and (x_h, y_h) can be extracted from the RD image. Then according to the above RD mapping, the observation matrix can be obtained for radar A as follows:

$$\mathbf{G}_A(t_m) = \mathbf{S}\mathbf{R}_A(t_m)\mathbf{C}, \quad (11)$$

where $\mathbf{G}_A(t_m)$ is the observation matrix composed of pulse time varied positions of scattering centers on the RD images, namely (X_A^i, Y_A^i) , (X_A^k, Y_A^k) and (X_A^h, Y_A^h) , \mathbf{C} is the configuration matrix composed of the relative positions of scattering centers on the physical plane,

$$\mathbf{G}_A(t_m) = \begin{bmatrix} X_A^i - X_A^h & X_A^i - X_A^k \\ Y_A^i - Y_A^h & Y_A^i - Y_A^k \end{bmatrix}, \quad \mathbf{C} = \begin{bmatrix} x_i - x_h & x_i - x_k \\ y_i - y_h & y_i - y_k \end{bmatrix} = \begin{bmatrix} x_1 & x_2 \\ y_1 & y_2 \end{bmatrix}. \quad (12)$$

The following observation matrix is provided by radar B,

$$\mathbf{G}_B(t_m) = \mathbf{S}\mathbf{R}_B(t_m)\mathbf{C}, \quad (13)$$

where $\mathbf{G}_B(t_m)$ is the corresponding observation matrix composed of pulse time varied positions of scattering centers on the RD image formed by radar B, namely (X_B^i, Y_B^i) , (X_B^k, Y_B^k) and (X_B^h, Y_B^h) ,

$$\mathbf{G}_B(t_m) = \begin{bmatrix} X_B^i - X_B^h & X_B^i - X_B^k \\ Y_B^i - Y_B^h & Y_B^i - Y_B^k \end{bmatrix}. \quad (14)$$

4.1 Rotating velocity estimation by a single radar

Suppose that three scattering centers can be extracted and correctly associated on two RD images formed at t_{m1} and t_{m2} . Then the equivalent rotating velocity of the target can be estimated by a single radar. The following discussion is based on the data collected by radar A, but it is also valid for the data collected by radar B. From eq. (11), it follows that

$$\mathbf{G}_{A2} = \mathbf{S}\mathbf{R}_A(t_{m2})\mathbf{R}_A^{-1}(t_{m1})\mathbf{S}^{-1}\mathbf{G}_{A1}, \quad (15)$$

where \mathbf{G}_{A1} and \mathbf{G}_{A2} are the observation matrices obtained at t_{m1} and t_{m2} , respectively.

Suppose that the inverse of the observation matrix \mathbf{G}_{A1} exists, which means the three scattering centers do not lie around a line as shown in Figure 2(a). Then

$$\mathbf{H}_{A-12} = \mathbf{G}_{A2}\mathbf{G}_{A1}^{-1} = \mathbf{S}\mathbf{R}_A(t_{m2})\mathbf{R}_A^{-1}(t_{m1})\mathbf{S}^{-1} = \begin{bmatrix} \cos \Delta\theta_{A12} & -(\eta_a/\eta_r) \sin \Delta\theta_{A12} \\ (\eta_r/\eta_a) \sin \Delta\theta_{A12} & \cos \Delta\theta_{A12} \end{bmatrix}, \quad (16)$$

where \mathbf{H}_{A-12} can be viewed as differential results of the observation at different times, and $\Delta\theta_{A12}$ is the AAD between two RD images,

$$\Delta\theta_{A12} = \theta_A(t_{m2}) - \theta_A(t_{m1}) = \omega_o(t_{m2} - t_{m1}). \quad (17)$$

For 2×2 matrix $\mathbf{M} = \begin{bmatrix} m_{11} & m_{12} \\ m_{21} & m_{22} \end{bmatrix}$, $\text{ted}()$ is defined as

$$\text{ted}(\mathbf{M}) = m_{11}m_{22} + m_{21}m_{12} \quad (18)$$

From eq. (16), it is easily understood that $\det(\mathbf{H}_{A-12}) = 1$ and

$$\text{ted}(\mathbf{H}_{A-12}) = \cos(2\Delta\theta_{A12}). \quad (19)$$

Then, the AAD between two RD images formed at t_{m1} and t_{m2} is estimated as

$$\Delta\theta_{A12} = 0.5\text{acos}(\text{ted}(\mathbf{H}_{A-12})) = 0.5\text{acos}(\text{ted}(\mathbf{H}_{A-12}) - \det(\mathbf{H}_{A-12}) + 1). \quad (20)$$

With the above AAD estimation and the known imaging time of these two RD images, the rotating velocity of the target is easily obtained.

4.2 Rotating center estimation

The estimation of the equivalent rotating center is required for the registration process in the subsequent image fusion [5]. By eqs. (4) and (6), the estimation of X_{AO} and X_{BO} actually provides the information of the rotating center [13]. For radar A, from eq. (4) we have

$$\begin{bmatrix} X_{A2}^n - X_{AO} \\ Y_{A2}^n - Y_{AO} \end{bmatrix} = \mathbf{H}_{A-12} \begin{bmatrix} X_{A1}^n - X_{AO} \\ Y_{A1}^n - Y_{AO} \end{bmatrix}, \quad (21)$$

where $Y_{AO} \approx 0$, (X_{A1}^n, Y_{A1}^n) and (X_{A2}^n, Y_{A2}^n) denote the positions of the n th scattering center on the RD images formed at t_{m1} and t_{m2} , respectively.

Thus, the equivalent rotating center is estimated as

$$\begin{bmatrix} X_{AO} \\ Y_{AO} \end{bmatrix} = (\mathbf{I} - \mathbf{H}_{A12})^{-1} \left\{ \begin{bmatrix} X_{A2}^n \\ Y_{A2}^n \end{bmatrix} - \mathbf{H}_{A12} \begin{bmatrix} X_{A1}^n \\ Y_{A1}^n \end{bmatrix} \right\}. \quad (22)$$

The equivalent rotating center can be estimated by radar B in the same way. As can be seen from the above discussion, the rotating center is estimated after the rotating velocity is available.

4.3 AAD estimation for different data collection planes

From eqs. (4)–(7), the observation matrices provided by radar A and radar B have the following relation:

$$\mathbf{G}_A(t_h) = \mathbf{S}\mathbf{R}_A(t_h)\mathbf{R}_B^{-1}(t_k)\mathbf{S}^{-1}\mathbf{G}_B(t_k), \quad (23)$$

where $h, k = 1, 2$.

When the inverse of matrix $\mathbf{G}_B(t_k)$ exists, we have

$$\mathbf{H}_{AB-hk} = \mathbf{G}_{Ah}\mathbf{G}_{Bk}^{-1} = \begin{bmatrix} \cos \Delta\theta_{AB-hk} & -(\eta_a/\eta_r) \sin \Delta\theta_{AB-hk} \\ (\eta_r/\eta_a) \sin \Delta\theta_{AB-hk} & \cos \Delta\theta_{AB-hk} \end{bmatrix}, \quad (24)$$

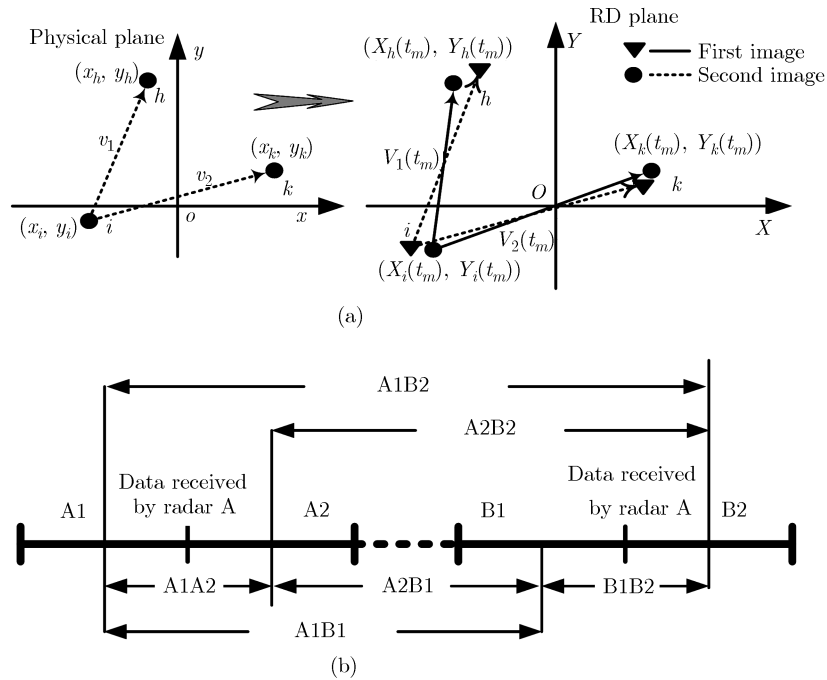


Figure 2 AAD estimation. (a) RD mapping; (b) AAD estimation scheme.

where the AAD $\Delta\theta_{AB_hk}$ is

$$\Delta\theta_{AB_hk} = \theta_A(t_h) - \theta_B(t_k) = \omega_o(t_h - t_k) - \beta_D. \tag{25}$$

Similar to eq. (20), the AAD between each two RD images can be estimated. When these two RD images are provided at the same time, the AAD between two radars is obtained. Combined with the system parameters and the AAD estimation at different times, the rotating velocity can also be estimated.

$$\Delta\theta_{AB_hk} = \omega_o(t_{mh} - t_{mk}) - \beta_D, \quad h, k = 1, 2. \tag{26}$$

4.4 Processing scheme of fused imaging by two aspect observations

Considering the characteristics of the proposed target's rotation and AAD estimation method, the key steps for the implementation of the proposed imaging scheme are given as follows.

First, after translational motion compensation, divide the received data equally into four RD images labeled as A1, A2, B1, and B2 as shown in Figure 2(b).

Second, extract relatively constant prominent scattering centers on each RD image using the weighting method [6, 13], and associate these scattering centers with the nearest neighboring method.

Third, estimate the AAD between each two of the above four RD images with the proposed method. Then, the rotating velocity of the target can be obtained.

At last, with the estimated rotating velocity of the target, cross-range scale the RD images to present the target in the homogeneous range cross-range domain, or use the CBP method to mitigate the migration of scattering centers through resolution cells (MTRC), and provide well focused images. Combined with AAD estimation between two radars, a fused imaging result is finally obtained by the CBP method.

As can be seen from Figure 2(b), with the estimation of AAD between A1 and A2, denoted by A1A2, the rotating velocity of the target is obtained with the known imaging intervals. What's more, the AAD between A1 and B1, or between A2 and B2, is actually the AAD between two radars. Note that the rotating velocity of the target can also be estimated by the AAD of the RD images from two radar systems, i.e., the AAD of A1B1 minus A2B1 and the AAD of A1B2 minus A2B2 can provide the AAD of A1A2. Also, the same method can be used to estimate the AAD of B1B2. At last, with the estimated rotating velocity, the rotating center of the target can be determined for each radar system. By combining

all AAD estimations, ref. [14] demonstrated that the rotation estimation by two radars is more accurate than that provided by a single radar through Monte Carlo trials.

5 Performance analysis

As mentioned above, the fused imaging with multi-aspect observations requires key information including the rotation of the target and the AAD between each data collection plane. According to the proposed method, the key information is provided by the estimation of the AAD between every two RD images. There are many factors that may affect the estimation of the AAD, such as the scintillation of scattering centers, the non-ideal translational motion compensation and the error in scattering centers' position extraction. In this section, the performance of AAD estimation is analyzed and the result shows how the proposed method is affected by some related factors.

Suppose two RD images are formed with the aspect angles being β_1 and β_2 , and $\Delta\theta_a = \beta_1 - \beta_2$ is the corresponding AAD. Thus, two observation matrices \mathbf{G}_1 and \mathbf{G}_2 are obtained from these two RD images. Because of the position extraction error of scattering centers, the observed matrices can be given by

$$\hat{\mathbf{G}}_m = \mathbf{G}_m + \mathbf{E}_m, \tag{27}$$

where the error matrices \mathbf{E}_m are composed of the position extraction error of the scattering centers,

$$\mathbf{E}_m = \begin{bmatrix} \varepsilon_{x_mi} - \varepsilon_{x_mh} & \varepsilon_{x_mi} - \varepsilon_{x_mk} \\ \varepsilon_{y_mi} - \varepsilon_{y_mh} & \varepsilon_{y_mi} - \varepsilon_{y_mk} \end{bmatrix} = \begin{bmatrix} \varepsilon_{m_11} & \varepsilon_{m_12} \\ \varepsilon_{m_21} & \varepsilon_{m_22} \end{bmatrix}. \tag{28}$$

The position extraction error of each scattering center is composed of the range error and Doppler error. Here, suppose the range error and Doppler error are independent. Also, suppose the position extraction error is independent for each different extraction of scattering centers. Then, the following statistics can be obtained:

$$E(\varepsilon_{1_ij}\varepsilon_{2_hk}) = 0, \quad E(\varepsilon_{m_1j}) = E(\varepsilon_{m_2j}) = 0, \quad m, i, j, h, k = 1, 2, \tag{29}$$

$$E(\varepsilon_{m_11}^2) = E(\varepsilon_{m_12}^2) = 2\sigma_x^2, \quad E(\varepsilon_{m_21}^2) = E(\varepsilon_{m_22}^2) = 2\sigma_y^2, \quad m = 1, 2, \tag{30}$$

$$E(\varepsilon_{m_11}\varepsilon_{m_12}) = \sigma_x^2, \quad E(\varepsilon_{m_21}\varepsilon_{m_22}) = \sigma_y^2. \tag{31}$$

With the above assumption, the resulting differential matrix \mathbf{H} is obtained as

$$\hat{\mathbf{H}} = \hat{\mathbf{G}}_1 \hat{\mathbf{G}}_2^{-1} = \begin{bmatrix} h_1 + \Delta h_1 & h_2 + \Delta h_2 \\ h_3 + \Delta h_3 & h_4 + \Delta h_4 \end{bmatrix}. \tag{32}$$

For the convenience of the performance analysis, the AAD estimation is accomplished with the second method in eq. (20). Then, define

$$f_d(\Delta\theta_a) = \cos(2\Delta\theta_a) = \text{ted}(\mathbf{H}) - \det(\mathbf{H}) + 1. \tag{33}$$

Thus, the function is evaluated as $\hat{f}_d(\Delta\theta_a)$ with the available $\hat{\mathbf{H}}$, which means that the error in the evaluation of this function is

$$\varepsilon_d(\Delta\theta_a) = \hat{f}_d(\Delta\theta_a) - f_d(\Delta\theta_a) = 2(h_3\Delta h_2 + h_2\Delta h_3 + \Delta h_2\Delta h_3). \tag{34}$$

Furthermore, function $f_d(\Delta\theta_a)$ can be expanded at a given point $\Delta\theta_{ao}$,

$$f_d(\Delta\theta_a) \approx \cos(2\Delta\theta_{ao}) - 2\sin(2\Delta\theta_{ao})\varepsilon_{dA}, \tag{35}$$

where $\varepsilon_{dA} = \Delta\theta_a - \Delta\theta_{ao}$.

Hence, the error in the estimation of AAD is expressed as

$$\varepsilon_{AE} = \Delta\hat{\theta}_a - \Delta\theta_a \approx \frac{\varepsilon_d(\Delta\theta_a)}{-2\sin(2\Delta\theta_a)}. \tag{36}$$

With the above analysis, the expectation and variance of ε_{AE} are finally obtained as

$$E(\varepsilon_{AE}) = 0, \quad (37)$$

$$\begin{aligned} \text{var}(\varepsilon_{AE}) = E(\varepsilon_{AE}^2) = & \frac{2K}{\sin^2(2\Delta\theta_a)} \{18K\hat{\sigma}_x^2\hat{\sigma}_y^2 + 6KP\hat{\sigma}_x\hat{\sigma}_y(\hat{\sigma}_x + \hat{\sigma}_y) \\ & + [2KP^2 + (3 - KP^2)\cos^2\Delta\theta_a]\hat{\sigma}_x\hat{\sigma}_y + \sin^2\Delta\theta_a[P(\hat{\sigma}_x + \hat{\sigma}_y) + 3(\hat{\sigma}_x^2 + \hat{\sigma}_y^2)]\}, \end{aligned} \quad (38)$$

where K and P are determined by the configuration triangle as shown in Figure 2(a), K is related to the area of the triangle and P is related to the side length of the triangle, $\hat{\sigma}_x$ and $\hat{\sigma}_y$ are determined by the range and cross range scaling factor of the RD image as well as the position extraction error of scattering centers,

$$P = (x_1^2 + x_2^2 - x_1x_2) + (y_1^2 + y_2^2 - y_1y_2), \quad K = 1/(x_1y_2 - x_2y_1)^2. \quad (39)$$

$$\hat{\sigma}_x = \eta_r^2\sigma_x^2, \quad \hat{\sigma}_y = \eta_a^2\sigma_y^2. \quad (40)$$

The above analysis shows that the proposed AAD estimation method relies on the position extraction and association of scattering centers from RD images formed at different aspects. In real applications, the scattering characteristics change with the aspect angle. However, in a limited span of the observation angle, relatively constant and prominent scattering centers can often be extracted especially for artificial targets. Thus, the above proposed AAD estimation method is well suitable for multi-aspect observations when the change in the aspect angles is limited within a relatively small range. Also, the effect of the scattering characteristics on the AAD estimation can be represented by the position extraction error of scattering centers. With the performance analysis, a reliable estimation for the AAD can be achieved by extracting as more scattering centers as possible on the RD images and making optimum combination of them.

6 Numerical experiments

In this section, the first part of numerical simulations are provided to demonstrate the performance of the proposed AAD estimation method. The second part of simulations are provided to demonstrate the effectiveness of the proposed imaging scheme with multi-aspect observations.

6.1 Monte Carlo trials for the performance of AAD estimation

Some Monte Carlo trials are performed in this section to give a more direct illustration of how the performance of the proposed AAD estimation is affected by relative factors. For the subsequent Monte Carlo trials, the default simulation parameters are set as follows. The default range and cross-range scaling factor are 0.375 and 0.531 m/pixel, respectively. The default root mean square error (RMSE) for 2D position extraction errors is set at $\sigma_x = \sigma_y = 0.1$ pixel, the AAD between two RD images is 3.0 deg, the two configuration vectors are 7 and 5 m long, respectively, and the angle between them is 50 deg. For each Monte Carlo trial, one of the parameters is varying, whereas the others maintain their default values. In addition, the RMSE of the AAD estimation versus a specified parameter, obtained by the analytic expression as eq. (38) and the Monte Carlo experiment, are given for simultaneous comparison.

The first experiment demonstrates how the RMSE for the estimation of $\Delta\theta_a$ changes with $\Delta\theta_a$ itself. It is obvious that the RMSE curve monotonically decreases with $\Delta\theta_a$, and the performance improves little when $\Delta\theta_a$ reaches a given value such as 2.0 deg in this case as shown in Figure 3(a).

The second experiment demonstrates how the RMSE for the estimation of $\Delta\theta_a$ changes with η_a . It is shown that the RMSE curve increases with η_a , meaning that finer image resolution provides better estimation for $\Delta\theta_a$ as shown in Figure 3(b).

The third experiment demonstrates how the RMSE for the estimation of $\Delta\theta_a$ changes with σ_x (σ_y). The RMSE curve increases with σ_x as shown in Figure 3(c). Thus, better extraction of scattering centers ensures better estimation for $\Delta\theta_a$.

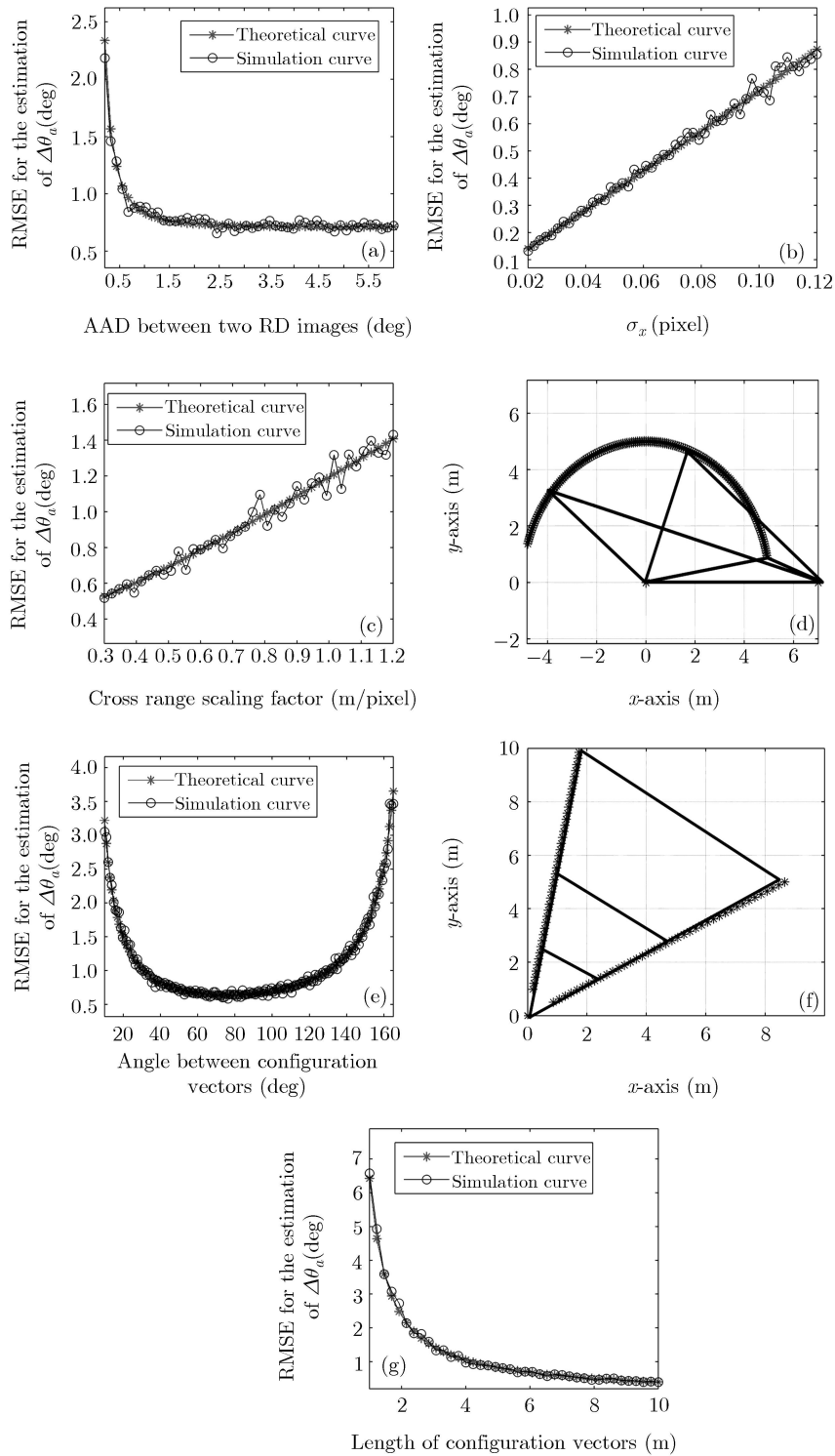


Figure 3 Performance simulation results. (a) RMSE for the estimation of $\Delta\theta_a$ varies with $\Delta\theta_a$; (b) RMSE for the estimation of $\Delta\theta_a$ varies with σ_x ; (c) RMSE for the estimation of $\Delta\theta_a$ varies with η_a ; (d) change the angle between two configuration vectors with their length fixed; (e) RMSE for the estimation of $\Delta\theta_a$ varies with angle between two configuration vectors; (f) change configuration vectors' length while the angle between them fixed; (g) RMSE for the estimation of $\Delta\theta_a$ varies with the length of configuration vectors.

In order to demonstrate how the configuration matrix affects the performance of the proposed method, the fourth experiment shows how the RMSE curve changes with the angle between two configuration vec-

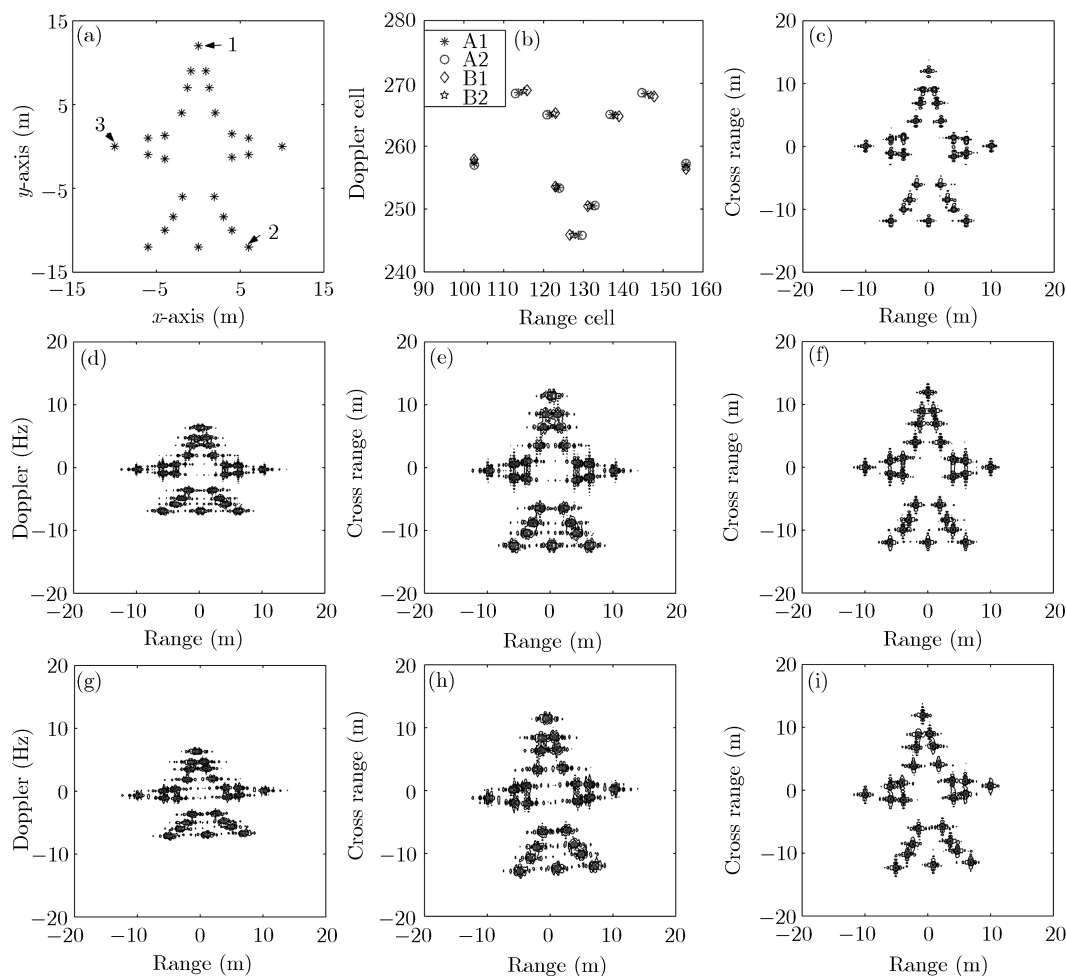


Figure 4 Imaging experiments. (a) Target model of scattering centers; (b) position extraction and association of scattering centers; (c) fused imaging result; (d) un-scaled RD imaging result by radar A; (e) cross range scaled RD imaging result by radar A; (f) CBP imaging result by radar A; (g) un-scaled RD imaging result by radar B; (h) cross range scaled RD imaging result by radar B; (i) CBP imaging result by radar B.

tors while their length is fixed as shown in Figure 3(d). As can be seen from Figure 3(e), good performance can be acquired when the angle between two configuration vectors is neither too small nor too large, which avoids ill-conditioned observation matrices. What's more, the fifth experiment increases the length of configuration vectors with the angle between them fixed as shown in Figure 3(f). It is obvious that the RMSE curve monotonically decreases with the increase of the configuration vectors' length as shown in Figure 3(g). These two experiments mean that the larger the relative distance of the three scattering centers, the better estimation for $\Delta\theta_a$ the proposed method can provide.

6.2 Fused imaging with data collected from two separated radars

In this imaging experiment, the main simulation parameters are given as follows. The systems transmit signals with a bandwidth of 300 MHz and a carrier frequency of 5.52 GHz. The pulse repetition frequency is 300 Hz, and the echoes are I/Q sampled with a sampling rate of 400 MHz. The AAD between two radars is set at 4 deg, and the target is made to rotate with a constant velocity of 0.015 rad/s. Each radar receives 1024 pulses, corresponding to an observation angle of about 2.93 deg, which means that the theoretical resolution of the image provided by a single radar is 0.5 m in the range direction and 0.531 m in the cross-range direction.

The target is composed of independent scattering centers as shown in Figure 4(a), and 9 scattering centers are extracted and associated with the proposed method in section 4 as shown in Figure 4(b).

Table 1 AAD estimation results

Unit: deg	A1	A2	
B1	4.0424	5.5300	1.4876
B2	2.5720	4.0605	1.4885
1.4562	1.4704	1.4695	1.4762

Table 2 Resolution calculation

Unit: m	Scatterer	RD image by A	CBP image by A	Fused image
RR	1	0.5469	0.4297	0.4297
	2	0.5469	0.4688	0.4297
	3	0.5078	0.4688	0.4688
CRR	1	0.5493	0.4944	0.2747
	2	0.4944	0.4999	0.1648
	3	0.5493	0.4944	0.2747

With the proposed method in this paper, the estimation for the AAD between every two RD images is given in Table 1. Thus, the AAD between the RD images A1 and A2 is estimated to be 1.4849 and 1.4562 deg between B1 and B2. Also, by combination of all the AAD estimation, the AAD between A1 and A2 are estimated to be 1.4876 and 1.4885 deg; and the AAD between B1 and B2 are estimated to be 1.4704 and 1.4695 deg, respectively. Thus, the target's rotating velocity is finally estimated to be 0.0151 rad/s.

Also, the AAD between A1 and B1 and the AAD between A2 and B2 are estimated to be 4.0424 and 4.0605 deg, respectively, leading to an average estimation of 4.0514 deg.

With the estimated rotating velocity, the RD imaging result by a single radar can be cross range scaled. Also, polar format algorithm (PFA) or CBP algorithm can be exploited to mitigate the MTRC of scattering centers and thus can provide finer focused imaging results. What's more, with the estimated AAD between two radars, a fused imaging result is obtained with much better resolution as shown in Figure 4.

Furthermore, the image contrast is calculated for the above imaging results. The RD image and CBP image with data provided by radar A have image contrast of 8.0565 and 10.1421, respectively. And the fused image has an image contrast of 12.7250. Also, the range resolution (RR) and cross range resolution (CRR) of three scattering centers are calculated in Table 2, which further demonstrates the effectiveness of the proposed method. As can be seen from Table 2, fusing processing mainly improves the cross range resolution of the target because the AAD between two radars is relatively small in this simulation.

7 Conclusions

Multi-aspect observations of a rotating target can provide imaging results with different target poses on them, and thus provides more information about the target being imaged. When the data collection planes of different aspect observations are coplanar, a fused imaging result may be obtained with finer resolution. With a two-ISAR configuration, this paper proposed a method to estimate the AAD between different data collection planes, as well as the rotation information of the target based on the extraction of scattering centers on different RD images. Also, the performance of the AAD estimation is analyzed, which helps to understand some relative factors that may affect the performance. All this paves a way for a more effective implementation of the proposed method. At last, after the required information is estimated, a fused imaging result is obtained with data collected by two radar systems. Numerical simulations are provided to demonstrate the effectiveness of the proposed method. Notably, the proposed method can also be generalized to other imaging configurations such as multi-static ISAR [11] and multi-aspect spotlight synthetic aperture radars [12].

Acknowledgements

This work was supported by the National Natural Science Foundation of China (Grant No. 60971087), China Ministry Research Foundation (Grant No. 9140A07011810JW01), the Aerospace Innovation Foundation (Grant No. CASC200904), and China Aviation Science Foundation (Grant No. 20080158001).

References

- 1 Walker J L. Range-Doppler imaging of rotating objects. *IEEE Trans Aerosp Electron Syst*, 1980, 16: 23–52
- 2 Wehner D, Barnes B. *High Resolution Radar*. 2nd ed. Norwood, MA: Artech House, 1994
- 3 Bao Z, Xing M D, Wang T. *Radar Imaging Technology* (in Chinese). Beijing: Publishing House of Electronics Industry, 2005
- 4 Voicu L I, Patton R, Myler H R. Multi-criterion vehicle pose estimation for SAR-ATR. In: *SPIE Conference on Algorithms for Synthetic Aperture Radar Imagery*, vol. VI, Denver, USA, 1999. 497–506
- 5 Li Z X, Papson S, Narayanan R M. Data-level fusion of multilook inverse synthetic aperture radar images. *IEEE Trans Geosci Remote Sens*, 2008, 46: 1394–1406
- 6 Liu F, Xu J D. Research on target identification with ISAR image sequence (in Chinese). *Modern Radar*, 2005, 27: 18–21
- 7 Wang G Y, Xia X G, Chen V C. Three-dimensional ISAR imaging of maneuvering targets using three receivers. *IEEE Trans Image Process*, 2001, 10: 436–446
- 8 Zhang Q, Yeo T S. Three-dimensional SAR imaging of a ground moving target using the InISAR technique. *IEEE Trans Geosci Remote Sens*, 2004, 42: 1818–1828
- 9 Burkholder R J, Gupta I J, Johnson J T. Comparison of monostatic and bistatic radar images. *IEEE Anten Propag Mag*, 2003, 45: 41–50
- 10 Palmer J, Homer J, Longstaff I D, et al. ISAR imaging using an emulated multistatic radar system. *IEEE Trans Aerosp Electron Syst*, 2005, 41: 1464–1472
- 11 Martorella M, Palmer J, Homer J, et al. On bistatic inverse synthetic aperture radar. *IEEE Trans Aerosp Electron Syst*, 2007, 43: 1125–1134
- 12 Jakowatz C V, Wahl D E, Eichel P H, et al. *Spotlight-mode Synthetic Aperture Radar: A Signal Processing Approach*. Boston: Kluwer Academic Publishers, 1996
- 13 Ye C M, Xu J, Zuo Y, et al. Rotating center estimation for inverse synthetic aperture radar imaging (in Chinese). *J Tsinghua Univ (Sci Tech)*, 2009, 49: 1205–1208
- 14 Ye C M, Xu J, Peng Y N, et al. Target rotating velocity estimation with bi-static ISAR (in Chinese). In: *Proceedings of the 10th Radar Conference*. Beijing: National Defense Industry Press, 2008